J. Fluid Mech. (1997), *vol.* 351, *pp.* 359–378. Printed in the United Kingdom

© 1997 Cambridge University Press

Mixed convection due to a finite horizontal flat plate embedded in a porous medium

By M. VYNNYCKY[1]† AND I. POP[2]

[1]Tohoku National Industrial Research Institute, 4-2-1 Nigatake, Miyagino-Ku, Sendai, 983 Japan
[2]University of Cluj, Faculty of Mathematics, R-3400 Cluj, CP 253 Romania

(Received 15 April 1996 and in revised form 13 June 1997)

Simultaneous steady forced and free convective flow past a heated or cooled body in a semi-infinite porous medium subject to the Darcy–Boussinesq approximation is treated analytically and numerically. A correction term is derived in terms of the Rayleigh (Ra) and Péclet (Pe) numbers for the velocity and temperature fields far from the body; this is subsequently implemented in a numerical treatment, using finite-difference techniques in elliptical coordinates, for $1 \leqslant Pe \leqslant 100$ and $|Ra| \leqslant 10^3$. Flow separation is observed for both heating and cooling, perhaps surprisingly so for the former case since the flow near the plate is being accelerated by comparison with the forced convection case. A simple analogy with inviscid flow theory serves to illustrate the manner in which separation eddies are formed for both heating and cooling cases.

1. Introduction

Fundamental studies related to thermal convection in porous media have increased significantly during recent years. The requirement for energy, the necessity to develop effective technologies for nuclear waste management, transpiration cooling, separation processes in chemical industries, building thermal insulations, winding structure for high-power density in electric machines, packed-bed catalytic reactors and numerous other applications have led to a considerable interest in convective heat transport through porous media, especially in the last three decades. The same processes are also found naturally within living organisms, such as in biological membranes and filters and the flow of blood or other body fluids. The abundance of these phenomena is due to the fact that the fluid trapped in the pores of the substance can be subjected to vaporization, condensation or to migration due to applied pressure gradients. Some of the early descriptions and results in this field can be found in the comprehensive reviews provided by Bejan (1984) and Kakac *et al.* (1991), and in the monographs by Nield & Bejan (1992) and Nakayama (1995).

The problem of thermal convection in porous media is mostly relevant to free convection flows from vertical and horizontal semi-infinite flat plates, which have become classical heat transfer problems in porous media. Cheng & Chang (1976) were probably the first to consider the free convection from a horizontal surface embedded in a porous medium, and much work has been done on this problem since. However, very little work exists in the literature on free convective heat transfer due

† Present address: Department of Mechanics, Royal Institute of Technology, S-100 44 Stockholm, Sweden.

to a finite-length vertical or horizontal surface. Using the scale analysis developed by Bejan (1984), Kimura, Bejan & Pop (1985) have studied analytically the heat and fluid flow features of the free convection boundary layer near a horizontal cold finite-length plate facing upwards and immersed in a porous medium. The boundary layer features were then confirmed in the Rayleigh number range $100 \leqslant Ra \leqslant 700$ by numerical solutions of the complete partial differential equations. Later, Merkin & Needham (1987) considered the boundary-layer natural convection above a heated short vertical wall embedded in a porous medium. It was shown that the boundary layers on each side of the wall merge to form a buoyant wake above the wall and that far downstream the flow is described by the two-dimensional wake solution. Most recently, Higuera & Weidman (1995) have considered flow in the free convection boundary layer below a downward-facing horizontal infinite strip and circular disk, subject to both constant temperature and constant heat flux conditions, in a porous medium; the analogous problem for the boundary-layer flow above a horizontal circular disk was treated earlier by Merkin & Pop (1989).

Despite its importance, few papers have treated the problem of combined forced and free convection (mixed convection) from a horizontal surface in a porous medium. As is known, thermal buoyancy effects can have a significant effect on the flow and heat transfer from a surface, either when the flow velocities are low or the temperature difference between the surface and external flow is high. Cheng (1977), Prasad, Lai & Kulacki (1988), Lai & Kulacki (1990), Aldoss, Chen & Armaly (1993*a, b*; 1994) and Aldoss, Jarrah & Duwari (1994) considered some aspects of this problem, such as the effect of a variable wall temperature distribution and mass flux (suction/injection) on the flow and heat transfer characteristics due to a surface embedded in a porous medium of infinite extent. On the other hand, Oosthuizen (1988) has investigated numerically mixed convective heat transfer due to a heated horizontal plate of finite length in a porous medium, mounted near an impermeable adiabatic horizontal surface.

The main purpose of this paper is to investigate mixed convective flow past the upper surface of a hot or cold body which is embedded in a fluid-saturated porous medium. It should be mentioned that the flow situation to be considered in this paper is analogous to the one studied by Robertson, Seinfeld & Leal (1973) for the classical viscous (non-porous) medium. Physically, this problem is motivated by its practical application in electronic cooling systems and geothermal areas which consist of troughs of volcanic debris or other heat sources; furthermore, the problem has relevance to the attempts to identify a geological repository for the storage of nuclear waste. First, we formulate the full two-dimensional time-independent problem for arbitrary body shape; then, for reasons of analytical expediency, bodies which are symmetric about the horizontal axis with antisymmetric temperature distributions are considered. On the way to providing a numerical solution to the full momentum and energy equations subject to the Darcy–Boussinesq approximation for a wide range of Rayleigh (Ra) and Péclet (Pe) numbers in the case of a finite horizontal plate, an analytical solution is derived for the forced convection limit ($Ra = 0$), which is subsequently used to verify the numerical code. Furthermore, a correction term for the temperature and streamfunction at infinity is also derived in order to improve the imposed boundary conditions there; this proves beneficial to the numerical method used, particularly for the case when the plate is cooled. For high enough values of Ra, flow separation is observed to occur, and heuristic considerations are given in order to clarify the mechanism for the onset of this separation.

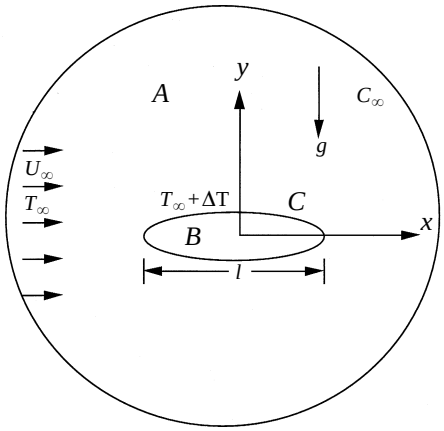

FIGURE 1. Sketch of the geometry for mixed convection.

2. Formulation

A schematic of the physical model and coordinate system is shown in figure 1. Consider a body B with boundary C of characteristic length l which is embedded in an infinite expanse of fluid-saturated porous medium at temperature T_∞, and assume that a uniform free stream with a velocity U_∞ is flowing parallel to the horizontal axis. The characteristic temperature of the body is taken to be $T_\infty + \Delta T$, with $\Delta T > 0$ for a heated body and $\Delta T < 0$ for a cold body. The buoyancy force associated with the temperature ΔT induces a streamwise pressure gradient which interacts with the forced convection flow adjacent to the plate. The pressure distribution across the flow is, however, not affected by the (mainly horizontal) motion of the fluid. Under this observation and the Darcy–Boussinesq approximation, the equations describing the steady motion can be written in non-dimensional form as

$$\nabla \cdot \boldsymbol{q} = 0. \tag{2.1a}$$

$$\boldsymbol{q} = -\nabla p + \frac{Ra}{Pe}\theta \boldsymbol{j}, \tag{2.1b}$$

$$\boldsymbol{q} \cdot \nabla\theta = \frac{1}{Pe}\nabla^2\theta. \tag{2.1c}$$

where $\boldsymbol{q}$ is the velocity vector, p is the pressure, θ is the temperature, $\boldsymbol{j}$ is the unit vector in the y-direction, ∇^2 is the Laplacian in regular Cartesian coordinates (x, y), and Ra and Pe are, respectively, the Rayleigh and Péclet numbers given by

$$Ra = \frac{g\beta K l \Delta T}{\alpha \nu}, \quad Pe = \frac{U_\infty l}{\alpha}. \tag{2.2a,b}$$

Here, g is the acceleration due to gravity, β the coefficient of thermal expansion, K the permeability of the porous medium, α the thermal diffusivity and ν the kinematic viscosity. The equations are non-dimensionalized using $U_\infty, (\mu l U_\infty / K), \Delta T$ and l as velocity, pressure, temperature and length scales, respectively, with μ being the dynamic viscosity.

The following boundary conditions are prescribed. At C, there is no normal fluid flow, so that

$$\boldsymbol{q} \cdot \boldsymbol{n} = 0; \tag{2.3}$$

here, $\boldsymbol{n}$ denotes the unit vector normal to C. In addition, the temperature is a

prescribed function θ_C, so that

$$\theta = \theta_C(x, y), \qquad \text{on} \qquad C. \tag{2.4}$$

As $x^2 + y^2 \to \infty$,

$$\boldsymbol{q} \to \boldsymbol{i}, \qquad p \to -x, \qquad \theta \to 0, \tag{2.5a–c}$$

where $\boldsymbol{i}$ denotes the unit vector in the x-direction. For later use, we also introduce the non-dimensional local Nusselt number Nu, defined by

$$Nu = -\left(\frac{\partial \theta}{\partial n}\right)_{n=0}, \tag{2.6}$$

with the overall Nusselt number $\overline{Nu}$, based on the total heat transfer at the body,

$$\overline{Nu} = \oint_C \left(\frac{\partial \theta}{\partial n}\right)_{n=0} \mathrm{d}s. \tag{2.7}$$

3. Analytical solution for the outer flow

In anticipation of the need to determine accurately the boundary conditions at infinity for the purposes of the numerical solution to come, we consider first the behaviour of the solution for the outer flow. Although our development has been quite general so far, certain restrictions will be in order, as follows. First, we apply Gauss's theorem to (2.1*b*) over the region A lying between the curves C and C_∞, as shown in figure 1. A little manipulation gives

$$-\oint_{C_\infty} \psi \, \mathrm{d}\boldsymbol{s} = -\boldsymbol{F} - \oint_{C_\infty} p \, \mathrm{d}\boldsymbol{n} + \left(\frac{Ra}{Pe} \int\int_A \theta \, \mathrm{d}A\right) \boldsymbol{j}, \tag{3.1}$$

where

$$\boldsymbol{F} = F_x \boldsymbol{i} + F_y \boldsymbol{j} = -\oint_C p \, \mathrm{d}\boldsymbol{n} \tag{3.2}$$

is the total force on the body; here, **s** denotes the unit vector tangential to C and ψ is the streamfunction defined by

$$u = \frac{\partial \psi}{\partial y}, \quad v = -\frac{\partial \psi}{\partial x}, \tag{3.3}$$

with u and v being the velocity components in the x- and y-directions respectively. To permit further asymptotic development, the body is taken to be symmetric, and θ antisymmetric, about $y = 0$; this ensures that the area integral vanishes, and that $\theta = 0$ on $y = 0$ outside the curve C. Furthermore, the body is now a heat dipole, and only the region $y > 0$ needs to be considered, although for the moment the integrals along the entire length of C and C_∞ will continue to be used, in order to exploit the similarities with the analysis of Chang (1961) for a viscous (non-porous) fluid. Introducing an artificial parameter ϵ, the following expansions for ϵ small are proposed.

3.1. *Outer expansion*

In the outer region, the independent variables are assumed to be of the form

$$\tilde{x} = \epsilon x, \quad \tilde{y} = \epsilon y, \tag{3.4}$$

so that equations (2.1*a–c*) become

$$\nabla \cdot \boldsymbol{q} = 0, \tag{3.5a}$$

$$\boldsymbol{q} = -\epsilon \nabla p + \frac{Ra}{Pe}\theta \boldsymbol{j}, \tag{3.5b}$$

$$\boldsymbol{q} \cdot \nabla \theta = \frac{\epsilon}{Pe}\nabla^2 \theta. \tag{3.5c}$$

The expansions for the outer dependent variables are assumed to have the form

$$\boldsymbol{q} = \boldsymbol{i} + \epsilon^2 \tilde{\boldsymbol{q}}_1 + o(\epsilon^2), \tag{3.6a}$$

$$p = -\frac{\tilde{x}}{\epsilon} + \epsilon \tilde{p}_1 + o(\epsilon), \tag{3.6b}$$

$$\theta = \epsilon^2 \tilde{\theta}_1 + o(\epsilon^2). \tag{3.6c}$$

3.2. *Inner expansion*

In the wake region, the independent variables are taken to be

$$\bar{x} = \tilde{x}, \quad \bar{y} = \frac{\tilde{y}}{\epsilon^{1/2}} = \epsilon^{1/2} y \tag{3.7}$$

and the dependent variables

$$u, \quad \bar{v} = \frac{v}{\epsilon^{1/2}}, \quad p \qquad \text{and} \qquad \theta. \tag{3.8}$$

Expressed in inner variables, the governing equations (2.1*a–c*) transform to

$$\frac{\partial u}{\partial \bar{x}} + \frac{\partial \bar{v}}{\partial \bar{y}} = 0, \tag{3.9a}$$

$$u = -\epsilon \frac{\partial p}{\partial \bar{x}}, \tag{3.9b}$$

$$\bar{v} = -\frac{\partial p}{\partial \bar{y}} + \frac{Ra}{Pe\epsilon^{1/2}}\theta, \tag{3.9c}$$

$$u\frac{\partial \theta}{\partial \bar{x}} + \bar{v}\frac{\partial \theta}{\partial \bar{y}} = \frac{1}{Pe}\left(\epsilon \frac{\partial^2 \theta}{\partial \bar{x}^2} + \frac{\partial^2 \theta}{\partial \bar{y}^2}\right). \tag{3.9d}$$

The inner expansions for the dependent variables are assumed to have the form

$$u \sim 1 + \epsilon^{3/2} u_1 + o(\epsilon^{3/2}), \tag{3.10a}$$

$$\bar{v} \sim \epsilon^{3/2} v_1 + o(\epsilon^{3/2}), \tag{3.10b}$$

$$p \sim -\frac{\bar{x}}{\epsilon} + \epsilon^{1/2} p_1 + o(\epsilon^{1/2}), \tag{3.10c}$$

$$\theta \sim \epsilon \theta_1 + o(\epsilon). \tag{3.10d}$$

3.3. *Solution for the wake region*

Considering the wake region first, (3.9*a–d*) reduce, at leading order, to

$$\frac{\partial u_1}{\partial \bar{x}} + \frac{\partial v_1}{\partial \bar{y}} = 0, \tag{3.11a}$$

$$u_1 = -\frac{\partial p_1}{\partial \bar{x}}, \tag{3.11b}$$

$$0 = -\frac{\partial p_1}{\partial \bar{y}} + \frac{Ra}{Pe}\theta_1, \tag{3.11c}$$

$$\frac{\partial \theta_1}{\partial \bar{x}} = \frac{1}{Pe}\frac{\partial^2 \theta_1}{\partial \bar{y}^2}, \tag{3.11d}$$

where the boundary conditions for θ_1 are $\theta_1 = 0$ on $\bar{y} = 0$ and $\theta_1 \to 0$ as $\bar{y} \to \infty$. Before writing down the solution, we note here that multiplying (3.11) by $\bar{y}$ and integrating across the wake gives that $\int_0^\infty \bar{y}\theta_1 \mathrm{d}\bar{y}$ (and hence $\int_0^\infty y\theta \mathrm{d}y$) are conserved; further, since $y \sim x^{1/2}$ in the wake, we have that θ should decay as $1/x$ there.

The appropriate solution to (3.11d) is then

$$\theta_1(\bar{x}, \bar{y}) = \bar{A}\bar{y}\bar{x}^{-3/2}\mathrm{e}^{-Pe\bar{y}^2/4\bar{x}}, \tag{3.12}$$

which is a consequence of the fact that, for both porous medium and fluid, the velocity field at infinity is a uniform stream. The constant $\bar{A}$ is related to the temperature field by

$$\bar{A} = -\lim_{x_0 \to \infty} \frac{x_0^{1/2}}{2} \int_{-x_0}^{x_0} \left(\frac{\partial \theta}{\partial y}\right)_{y=0} \mathrm{d}x, \tag{3.13}$$

which may be rewritten as

$$\bar{A} = \lim_{x_0 \to \infty} \frac{x_0^{1/2}}{2} \left(\overline{Nu}_+ - \int_{-x_0}^{X_-} \left(\frac{\partial \theta}{\partial y}\right)_{y=0} \mathrm{d}x - \int_{X_+}^{x_0} \left(\frac{\partial \theta}{\partial y}\right)_{y=0} \mathrm{d}x \right), \tag{3.14}$$

where $\overline{Nu}_+$ is the overall Nusselt number based on the heat transfer at the upper surface,

$$\overline{Nu}_+ = -\int_{C_+} \left(\frac{\partial \theta}{\partial n}\right)_{n=0} \mathrm{d}x, \tag{3.15}$$

and X_- and X_+ are respectively the x-coordinates of the extreme left- and right-hand endpoints of the body on $y = 0$. Equation (3.14) is obtained by considering the integral of (2.1c) over a semi-circle of radius x_0 centred at the origin, the upper part, C_+, of the curve C and the adjoining line segments between them. Note, incidentally, that we should expect $\bar{A} \neq 0$, even as $x_0 \to \infty$, a behaviour which runs counter to that stated by Robertson *et al.* (1973); we return to this point in §4.2. Further, we put

$$\tilde{\psi} = \epsilon\psi, \quad \bar{\psi} = \epsilon^{1/2}\psi \tag{3.16}$$

for the outer and inner streamfunctions, and take the expansions

$$\tilde{\psi} = \tilde{y} + \epsilon^2\tilde{\psi}_1 + o(\epsilon^2), \tag{3.17a}$$

$$\bar{\psi} = \bar{y} + \epsilon^{3/2}\bar{\psi}_1 + o(\epsilon^{3/2}), \tag{3.17b}$$

where $\tilde{\psi}_1$ and $\bar{\psi}_1$ are defined according to (3.3). Now, cross-differentiating (3.11b, c) to eliminate p_1, we obtain

$$\frac{\partial^2 \bar{\psi}_1}{\partial \bar{y}^2} = -\frac{Ra}{Pe}\frac{\partial \theta_1}{\partial \bar{x}}. \tag{3.18}$$

The solution to (3.18), subject to the requirement that $\bar{\psi}_1$ is finite as $\bar{y} \to \infty$ and $\bar{\psi}_1 = 0$ on $\bar{y} = 0$, is

$$\bar{\psi}_1 = -\frac{Ra}{Pe^2}\theta_1, \tag{3.19}$$

with the pressure p_1 given by

$$p_1 = \frac{2Ra\bar{A}}{Pe^2}\frac{\mathrm{e}^{-Pe\bar{y}^2/4\bar{x}}}{\bar{x}^{1/2}}. \tag{3.20}$$

3.4. *Solution external to the wake*

Outside the wake region, from (3.5*a–c*) and (3.6*a–c*), it follows that, to leading order,

$$\nabla\cdot\tilde{\boldsymbol{q}}_1 = 0, \tag{3.21a}$$

$$\tilde{\boldsymbol{q}}_1 = -\nabla\tilde{p}_1 + \frac{Ra}{Pe}\tilde{\theta}_1\boldsymbol{j}, \tag{3.21b}$$

$$\frac{\partial\tilde{\theta}_1}{\partial\tilde{x}} = 0. \tag{3.21c}$$

Hence $\tilde{\theta}_1$ is constant along the lines $\tilde{y}$ =constant (the streamlines of the undisturbed flow). Furthermore, since the temperature is zero at upstream infinity, it follows that $\tilde{\theta}_1$ is zero. Thence, $\tilde{\boldsymbol{q}}_1$ is potential. Thus, equations (3.21*a*, *b*) give, after some algebra,

$$\tilde{\psi}_1 = \frac{C_1\tilde{y}}{\tilde{x}^2+\tilde{y}^2}, \qquad \tilde{p}_1 = \frac{C_1\tilde{x}}{\tilde{x}^2+\tilde{y}^2}, \tag{3.22a,b}$$

where C_1 is a constant. To evaluate C_1, we consider the momentum integral (3.1). Introducing a non-dimensional tensor $\boldsymbol{A}$, whose entries are

$$A_{11} = A_{22} = -p - x, \quad A_{12} = -A_{12} = \psi - y,$$

and a vector streamfunction

$$\boldsymbol{G}(Q) = \int_P^Q \boldsymbol{A}\,\mathrm{d}\boldsymbol{n},$$

$\boldsymbol{G}$ is made single-valued by slitting the plane along the positive x-axis; here P is a given fixed point whose position is irrelevant, whereas Q is any other point in the plane. Then,

$$\boldsymbol{F} = \boldsymbol{G}(x,0_+) - \boldsymbol{G}(x,0_-) \equiv \Delta\boldsymbol{G},$$

where equations equivalent to (4.37)–(4.39) from Chang (1961) hold, so that

$$\Delta\boldsymbol{G} = \oint_{C_\infty}\tilde{p}_1\,\mathrm{d}\boldsymbol{n} - \oint_{C_\infty}\tilde{\psi}_1\,\mathrm{d}\boldsymbol{s} + \left(\int_{-\infty}^{\infty} p_1\,\mathrm{d}\bar{y}\right)\boldsymbol{i}. \tag{3.23}$$

Inserting (3.20) and (3.22*a*,*b*) gives

$$F_x = 2\pi C_1 + \frac{4Ra\bar{A}\pi^{1/2}}{Pe^{5/2}}, \qquad F_y = 0. \tag{3.24a,b}$$

3.5. *Composite solution*

Finally, from the theory of composite expansions, summing the inner and outer expansions gives the following leading-order far-field corrections for θ and ψ:

$$\left.\begin{aligned} &\theta = 0, \quad x < 0, \\ &\theta \sim \bar{A}yx^{-3/2}\mathrm{e}^{-Pey^2/4x} + o(r^{-1/2}), \quad x > 0; \end{aligned}\right\} \tag{3.25}$$

and

$$\left.\begin{aligned} \psi &\sim y + \frac{C_1 y}{x^2+y^2} + o(r^{-1}), \quad x < 0, \\ \psi &\sim y - \frac{Ra}{Pe^2}\bar{A} y x^{-3/2} \mathrm{e}^{-Pey^2/4x} + \frac{C_1 y}{x^2+y^2} + o(r^{-1}), \quad x > 0. \end{aligned}\right\} \tag{3.26}$$

Equations (3.24*a*) and (3.26*a, b*) can be used to determine the constant C_1 when the heating body is either a flat plate or a circular cylinder, placed in a forced convection flow ($Ra = 0$). With $Ra = 0$, we have for the first case the exact solution

$$\psi = y, \quad p = -x, \tag{3.27}$$

for the velocity and pressure fields, whence $F_x = 0$, so that $C_1 = 0$ from (3.24*a*) in agreement with (3.26). For a circular cylinder,

$$\psi = \left(r - \frac{1}{r}\right)\sin\phi, \quad p = -\left(r + \frac{1}{r}\right)\cos\phi, \tag{3.28}$$

which gives $F_x = -2\pi$, and thence $C_1 = -1$, once again in agreement with (3.26); here, (r, ϕ) denote polar coordinates.

4. Solutions for an isothermal finite flat plate

The foregoing is applied to the case of a flat plate lying at $y = 0, -1/2 \leqslant x \leqslant 1/2$. In order to solve (2.1*a–c*) subject to boundary conditions (2.3)–(2.5) numerically, the equations are rewritten in elliptic coordinates (ξ, η) using the transformation

$$x = \tfrac{1}{2}\cosh\xi\cos\eta, \quad y = \tfrac{1}{2}\sinh\xi\sin\eta. \tag{4.1}$$

Equations (2.1*a–c*) then become

$$\frac{\partial^2\psi}{\partial\xi^2} + \frac{\partial^2\psi}{\partial\eta^2} = -\frac{Ra}{Pe}\left(s_2\frac{\partial\theta}{\partial\eta} - s_1\frac{\partial\theta}{\partial\xi}\right), \tag{4.2a}$$

$$\frac{\partial\psi}{\partial\eta}\frac{\partial\theta}{\partial\xi} - \frac{\partial\psi}{\partial\xi}\frac{\partial\theta}{\partial\eta} = \frac{1}{Pe}\left(\frac{\partial^2\theta}{\partial\xi^2} + \frac{\partial^2\theta}{\partial\eta^2}\right), \tag{4.2b}$$

where

$$\left.\begin{aligned} &s_1 = \sinh\xi\cos\eta, \quad s_2 = \cosh\xi\sin\eta, \\ &J^2(\xi,\eta) = \tfrac{1}{2}(\cosh 2\xi - \cos 2\eta). \end{aligned}\right\} \tag{4.3}$$

The velocity components are given in these coordinates by

$$u = \frac{2}{J^2}\left(s_2\frac{\partial\psi}{\partial\xi} + s_1\frac{\partial\psi}{\partial\eta}\right), \qquad v = \frac{2}{J^2}\left(s_1\frac{\partial\psi}{\partial\xi} - s_2\frac{\partial\psi}{\partial\eta}\right). \tag{4.4a, b}$$

Furthermore, the plate is located at $\xi = 0$, and the remaining portions of the x-axis ($|x| > 1/2, y = 0$) are given by $\eta = 0 (x > 1/2)$ and $\eta = \pi (x < -1/2)$. We consider an isothermal plate, so that in (2.4) we set $\theta_C \equiv 1$. Thus the boundary conditions (2.3)–(2.5) become

$$\psi = 0, \quad \theta = 0 \qquad \text{on} \qquad \eta = 0, \pi, \quad \xi > 0, \tag{4.5a, b}$$

$$\psi = 0, \quad \theta = 1 \qquad \text{on} \qquad \xi = 0, \quad 0 \leqslant \eta \leqslant \pi, \tag{4.6a, b}$$

with the conditions at infinity given by

$$\left.\begin{aligned} &\theta = 0, \quad \pi/2 \leqslant \eta \leqslant \pi, \quad \xi \to \infty \\ &\theta \sim \bar{A} y x^{-3/2} \mathrm{e}^{-Pey^2/4x} + o(r^{-\frac{1}{2}}), \quad 0 \leqslant \eta < \pi/2, \quad \xi \to \infty, \end{aligned}\right\} \tag{4.7}$$

and

$$\left.\begin{aligned} &\psi \sim y + \frac{C_1 y}{x^2 + y^2} + o(r^{-1}), \quad \pi/2 \leqslant \eta \leqslant \pi, \quad \xi \to \infty \\ &\psi \sim y - \frac{Ra}{Pe^2} \bar{A} y x^{-3/2} \mathrm{e}^{-Pey^2/4x} + \frac{C_1 y}{x^2 + y^2} + o(r^{-1}), \quad 0 \leqslant \eta < \pi/2, \quad \xi \to \infty. \end{aligned}\right\} \tag{4.8}$$

In these coordinates, the non-dimensional local Nusselt number on the upper side of the plate, Nu_+, is

$$Nu_+ = -\frac{2}{\sin \xi} \left(\frac{\partial \theta}{\partial \xi} \right)_{\xi = 0}, \tag{4.9}$$

with the overall Nusselt number $\overline{Nu}_+$,

$$\overline{Nu}_+ = \int_0^{\pi} \left(\frac{\partial \theta}{\partial \xi} \right)_{\xi = 0} \mathrm{d}\eta. \tag{4.10}$$

To determine the constants C_1 and $\bar{A}$, note first that for this geometry $F_x = 0$ even when $Ra \neq 0$, because the integral in p at the plate surface in (3.1) vanishes, so that

$$C_1 = -\frac{2Ra\bar{A}}{Pe^{5/2} \pi^{1/2}}. \tag{4.11}$$

$\bar{A}$ itself, however, poses greater difficulties. Consideration of the closed-form solution of (2.1*a–c*) that is available when $Ra = 0$ for arbitrary Pe (see the Appendix for details) indicates, from the behaviour of the modified Bessel function K_1, that

$$\frac{\partial \theta}{\partial y} \sim \frac{1}{\pi(x + \frac{1}{2})} \qquad \text{as} \qquad x \downarrow -\tfrac{1}{2}, \tag{4.12a}$$

$$\frac{\partial \theta}{\partial y} \sim \frac{1}{\pi(\frac{1}{2} - x)} \qquad \text{as} \qquad x \uparrow \tfrac{1}{2}, \tag{4.12b}$$

so that Nu_+, as defined by (4.9), is non-integrable; furthermore, since the boundary conditions for θ are discontinuous at $x = \mp 1/2$ respectively, we may expect this situation to persist for $Ra \neq 0$, and it is worth exploring, at least heuristically, the nature of the singularities in this case.

Introducing an artificial parameter $\gamma (\ll 1)$, we consider, without loss of generality, the point at $(1/2, 0)$. Using rescaled Cartesian coordinates (X, Y) centred on this point, which are related to (x, y) by

$$x = \tfrac{1}{2} + \gamma X, \quad y = \gamma Y,$$

the governing equations reduce locally to

$$\frac{\partial^2 \psi}{\partial X^2} + \frac{\partial^2 \psi}{\partial Y^2} = -\gamma \frac{Ra}{Pe} \frac{\partial \theta}{\partial X}, \tag{4.13a}$$

$$\frac{\partial \psi}{\partial Y} \frac{\partial \theta}{\partial X} - \frac{\partial \psi}{\partial Y} \frac{\partial \theta}{\partial X} = \frac{1}{Pe} \left(\frac{\partial^2 \theta}{\partial X^2} + \frac{\partial^2 \theta}{\partial Y^2} \right). \tag{4.13b}$$

In view of the boundary conditions on θ on $Y = 0$, it is clear that we require $\theta \sim 1$,

in which case we must have either $\psi \sim \gamma$ or $\psi \sim 1$. In the first case, we arrive at just the conduction equation for θ, so that

$$\theta \sim \frac{1}{\pi} \tan^{-1}\left(\frac{Y}{X}\right), \tag{4.14}$$

whilst the second case gives

$$\psi \sim Y, \tag{4.15a}$$

$$\frac{\partial \theta}{\partial X} \sim \frac{1}{Pe}\left(\frac{\partial^2 \theta}{\partial X^2} + \frac{\partial^2 \theta}{\partial Y^2}\right). \tag{4.15b}$$

In either case, the key feature is that

$$\frac{\partial \theta}{\partial Y} \sim \frac{1}{\pi X} \qquad \text{near} \qquad X = 0,$$

so that the singularity in heat flux depends neither on Ra nor on Pe. Consequently, it is possible to take account of the singularity analytically by decomposing $\theta (\equiv \theta_s + \theta_f)$ into the sum of a component (θ_s) whose derivative with respect to y has a singularity near $x = \mp 1/2$, and whose integral along the x-axis will have a principal value, and a second component (θ_f) which is free of singularities and is integrable in the ordinary sense. For θ_s we can either choose a linear sum of terms which have the form (4.14), or the forced convection solution (A 5); we have chosen the latter. The prescription for $\bar{A}$ given by (3.14) now contains a principal-value integral, in the form

$$\bar{A} = -\lim_{x_0 \to \infty} \frac{x_0^{1/2}}{2} \fint_{-x_0}^{x_0} \left(\frac{\partial \theta}{\partial y}\right)_{y=0} \mathrm{d}x; \tag{4.16}$$

moreover, heat balance considerations when $Ra = 0$ give

$$\fint_{-\infty}^{\infty} \left(\frac{\partial \theta_s}{\partial y}\right)_{y=0} \mathrm{d}x = 0, \tag{4.17}$$

so that (4.16) becomes, on manipulating (3.14),

$$\bar{A} = \lim_{x_0 \to \infty} \frac{x_0^{1/2}}{2} \left(\int_{x_0}^{\infty} \left(\frac{\partial \theta_s}{\partial y}\right)_{y=0} \mathrm{d}x + \int_{-\infty}^{-x_0} \left(\frac{\partial \theta_s}{\partial y}\right)_{y=0} \mathrm{d}x - \int_{-x_0}^{x_0} \left(\frac{\partial \theta_f}{\partial y}\right)_{y=0} \mathrm{d}x \right), \tag{4.18}$$

which consists of well-behaved integrals only.

4.1. *Details of the numerical method*

With these modifications, (4.2*a*, *b*) for ψ and θ_f, subject to the boundary conditions (4.6)–(4.8), were solved numerically in the (η, ξ)-plane using a control-volume approach for the heat equation (Patankar 1980) and regular five-point differencing for the streamfunction equation; the resulting equations were swept over simultaneously and solved using Gauss–Seidel iteration with a convergence criterion given by

$$\max_{i,j} \left(|\psi_{i,j}^{(m)} - \psi_{i,j}^{(m-1)}|, |\theta_{i,j}^{(m)} - \theta_{i,j}^{(m-1)}| \right) < 10^{-8},$$

where m denotes the iteration order, and i and j are indices over η and ξ, respectively. In general, relaxation parameters of 1.8 and 0.7 were used for (4.2*a*, *b*) respectively, and all calculations required of the order of a few minutes on a Cray Supercomputer. Note, incidentally, that the technique employed is a modification of one that has been

	$Pe = 5$	$Pe = 10$	$Pe = 50$
Cheng (1977)	2.523	3.568	7.977
Prasad *et al.* (1988)	2.792	3.803	8.376
Present			
61×120	2.642	3.654	7.992
91×120	2.642	3.654	7.994
91×150	2.642	3.654	8.003

TABLE 1. Comparison of $\overline{Nu}_+$ values for $Ra = 0$ (zero heat flux for $|x| > 1/2$)

often used in recent years in conjugate heat transfer problems by Kimura & Pop (1992, 1993, 1994) and Vynnycky & Kimura (1994, 1995, 1996), the novel features here being the treatment of the singularities at the plate endpoints and the coupling of the inner flow with the boundary conditions at infinity. In particular, the outer boundary conditions were set, using (4.7) and (4.8) at a finite distance from the body, as indicated in the next paragraph; furthermore, since these outer conditions contain constants which depend on the solution near the surface of the body, the conditions themselves were updated, via (4.11) and (4.18), after each sweep as soon as the latest values for the flow variables became known.

To check our numerical method, we first set $Ra = 0$ to obtain converged solutions in the forced convection limit for a range of values of Pe; for these computations, we set the outer boundary conditions at $\xi_\infty = \cosh^{-1}(2x_\infty)$, with $x_\infty = 23.2$, and solved for θ and ψ, whereas for the later $Ra \neq 0$ computations, we solved for $\psi - y$ and $\theta_f (= \theta - \theta_s)$. Next, we replaced boundary condition (4.5*b*) with a zero flux condition in order to compare with results available in the literature (Cheng 1977; Prasad *et al.* 1988); the comparison is given in terms of $\overline{Nu}_+$ in table 1 for a set of three Pe values and uniform meshes and indicates that our results satisfactorily fall between values obtained earlier. The comparison in terms of $\overline{Nu}_+$ in this case is unambiguous, incidentally, because the singularities in Nu_+ at $x = \mp 1/2$ are of the form $(x \pm 1/2)^{-1/2}$ and hence integrable, as can be shown using Wiener–Hopf techniques (cf. Carrier, Crook & Pearson 1983, p. 376). Furthermore, we note that Cheng's (1977) similarity solution for forced convection on an isothermal horizontal surface,

$$\theta(X, Y) = \operatorname{erfc}\left(\frac{Y}{X^{1/2}}\right), \tag{4.19}$$

where $Y = Pe^{1/2} y, X = x + \frac{1}{2}$, is in fact the high-$Pe$ limit of the formulation with zero heat flux for $|x| > 1/2$, but not of that with zero temperature for $|x| > 1/2$.

Adopting the convention that $Ra > 0$ denotes a heated plate, and $Ra < 0$ a cooled plate, we proceed to a discussion for $Ra \neq 0$. Preliminary computations were carried out for $1 \leqslant Pe \leqslant 100$, $|Ra| \leqslant 10^3$ in order to ascertain the range over which the results of the numerical method would be valid. For instance, it is already known (Robertson *et al.* 1973) that in the computation of mixed convective flows for the case of a cooled plate immersed in a Newtonian fluid, the buoyancy force exerts a significant influence on the uniform flow boundary conditions at upstream infinity if x_∞ is not taken sufficiently large; on the other hand, the validity of the downstream infinity boundary conditions is in doubt when the plate is heated if Ra/Pe is too great (Prasad *et al.* 1988). Furthermore, the energy-balance method that is usually invoked to verify that the obtained numerical solution conserves heat runs into an ambiguity,

as follows. Applying the divergence theorem to (4.2*b*), we arrive at

$$\frac{1}{Pe}\left(\int_0^{\pi}\left(\frac{\partial\theta_f}{\partial\xi}\right)_{\xi=0}\mathrm{d}\eta \pm I(x_\infty)\right) = -\int_0^{\pi}\left(\theta\frac{\partial\psi}{\partial\eta} - \frac{1}{Pe}\frac{\partial\theta}{\partial\xi}\right)_{\xi=\xi_\infty}\mathrm{d}\eta$$
$$+\frac{1}{Pe}\left(\int_0^{\xi_\infty}\left(\frac{\partial\theta_f}{\partial\eta}\right)_{\eta=\frac{\pi}{2}}\mathrm{d}\xi - \int_0^{\xi_\infty}\left(\frac{\partial\theta_f}{\partial\eta}\right)_{\eta=0}\mathrm{d}\xi\right), \qquad (4.20)$$

where

$$I(x_\infty) = \frac{2}{\pi}\left(\cosh\tfrac{1}{2}Pe(x_\infty+\tfrac{1}{2}) - \cosh\tfrac{1}{2}Pe(x_\infty-\tfrac{1}{2}) - 2\int_{Pe/2(x_\infty-1/2)}^{Pe/2(x_\infty+1/2)}K_0(s)\sinh s\,\mathrm{d}s\right) \qquad (4.21)$$

denotes the value of the principal-value integral. However, it does not appear possible to calculate a percentage difference in energy based on the energy lost at the plate and the heat removed elsewhere plus that carried away downstream, since this would involve splitting up the integral of $(\partial\theta_s/\partial y)_{y=0}$. It was found, however, that the rearrangement shown in (4.20) gave a percentage difference of 2% or less for $Pe \geqslant 5$, although, in view of this arbitrariness, we chose not to rule out solutions for $Pe = 1$ for which this nominal difference was as high as 10%. Subsequently, all computations were carried out on the 91×150 mesh (the first quantity here denoting the number of points in the η-direction) using $x_\infty = 23.2$.

4.2. *Effect of Ra and Pe on flow structure*

Numerical solutions were obtained for $Pe = 1$, 5, 10, 50, 100, although not in all cases were we able to obtain solutions for $|Ra| = 10^3$. Figure 2 for $Pe = 5$ is typical of the streamline and isotherm plots that were obtained as the value of Ra/Pe was increased from negative to positive values. Figure 2(*d*) represents pure forced convection, whereas figure 2(*e*) for $Ra/Pe = 10$ illustrates an acceleration of the flow near the plate, as evidenced by the clustering of streamlines and the displacement of isotherms further downstream in figure 2(*e*). An additional feature here, not reported for the corresponding problem in a Newtonian fluid (Robertson *et al.* 1973), is the appearance of a separation bubble towards the trailing edge of the plate which reattaches to the x-axis further downstream beyond the trailing edge. This appears when $Ra/Pe > 0$, but is still not so large that the magnitude of the buoyancy force wrecks the uniform-stream assumption at downstream infinity; in fact, for $Pe = 5$, we were unable to obtain converged solutions for Ra much greater than 50. For $Ra/Pe < 0$, the gravitationally induced streamwise pressure gradient produces a deceleration of the flow near the plate, to the extent that the flow separates and a recirculating eddy, whose length increases with $-Ra/Pe$, forms. Whilst the location of the leading edge of the eddy continues to move upstream as $-Ra/Pe$ increases, the position of the eddy's trailing edge was noted to move downstream, but never to exceed $x = 0$. In addition, figure 3(*a–c*) indicates the extent to which the flow has been decelerated by comparison with figure 3(*d*) in that the isotherms have been compressed to lie within an ever smaller vicinity of the plate.

The effect of Ra and Ra/Pe on local heat transfer at the plate is shown in figures 3(*a*) and 3(*b*) for $Pe = 5$ and 100 respectively; to facilitate comparison, we have taken $|Nu_+|$ for the y-axis. In comparing the two plots, we note the development of a thermal boundary layer as Pe increases for $Ra = 0$, with a corresponding rise in Nu_+ values and increase in the asymmetry of the Nu_+ profile about $x = 0$; consequently, the

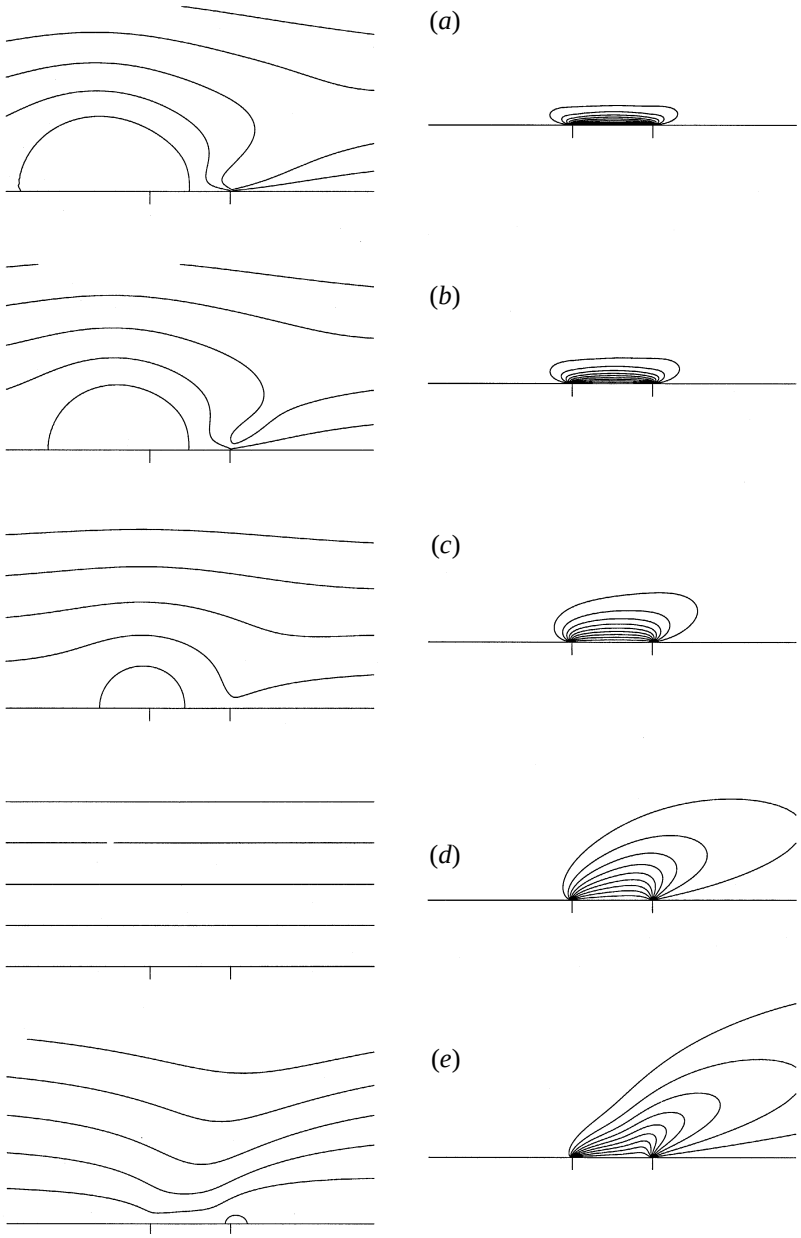

FIGURE 2. Streamlines, $0 \leqslant \psi \leqslant 5$ ($\Delta\psi = 0.5$) (left-hand plots), and isotherms, $0 \leqslant \theta \leqslant 1$ ($\Delta\theta = 0.1$) (right-hand plots) for $Pe = 5$: (*a*) $Ra/Pe = -200$; (*b*) $Ra/Pe = -100$; (*c*) $Ra/Pe = -50$; (*d*) $Ra/Pe = 0$; (*e*) $Ra/Pe = 10$. Ticks mark the leading and trailing edges of the plate at $x = \pm 1/2$, respectively; identical scales are used for both x- and y-directions.

sharp rise in Nu_+ near the trailing edge, as a result of the approaching discontinuity in the boundary condition, is more pronounced for the higher value of Pe. A more significant feature of note, which is more evident in figure 3(*a*) than in figure 3(*b*), is that for some negative values of Ra/Pe, the heat flux towards the plate is higher than for the pure forced convection solution. For $-Ra$ very large and positive, this is not surprising since it implies that the heat transfer as a result of natural convection is

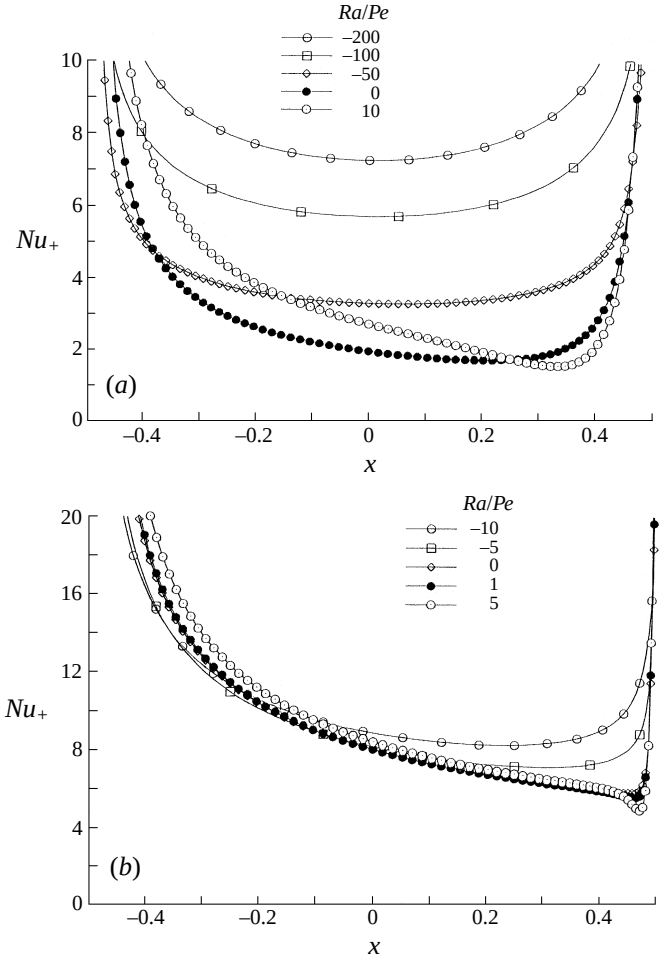

FIGURE 3. Nu_+ as a function of length along the plate for a selection of Ra/Pe values at (*a*) $Pe = 5$, (*b*) $Pe = 100$.

now more effective than that due to forced convection for that value of Pe. However, it is apparent from figure 3(*a*) that this situation persists even for $-Ra$ as low as 250, which is perhaps surprising in view of the general discussion on flow deceleration for negative Ra. On closer inspection, though, we do in fact observe flow deceleration in the vicinity of the leading edge, as evidenced by the lower values of Nu_+, by comparison with the $Ra = 0$ solution. Furthermore, we note that even though the plate is being cooled, the trailing edge nevertheless serves to accelerate the flow there (since locally $\partial\theta/\partial x > 0$); therefore, it appears that this effect, in addition to the forced flow, maintains the value of Nu_+ at a greater value for $Ra < 0$ than $Ra = 0$ for a major portion of the plate. For $Ra > 0$, which is thought of as the flow-accelerating case, one might therefore be surprised to see Nu_+ lower than for $Ra = 0$, as is the case for $Ra/Pe = 10$ in figure 3(*a*) in the vicinity of the trailing edge; however, a consideration of the local flow behaviour at different points of the plate, along the same lines as for $Ra < 0$, indicates this picture to be correct.

The flow development for a wide range of Ra and Pe values is illustrated in terms of the constant $\bar{A}$ in figure 4; for computing $\bar{A}$, we have taken $x_0 = x_\infty$ in (3.13). Since

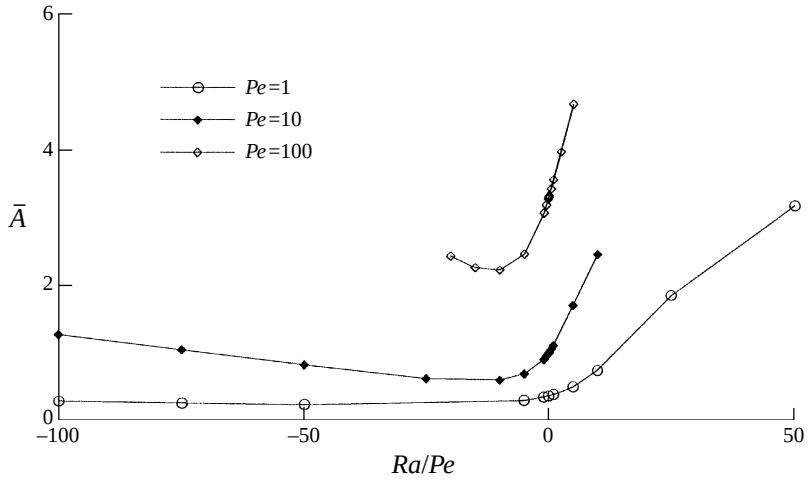

FIGURE 4. $\bar{A}$ as a function of Ra/Pe for $Pe = 1$, 10 and 100 for $x_0(= x_\infty) = 23.2$.

$\bar{A}$ may be thought of as the excess heat that is carried to downstream infinity, we may note from this figure how, for $Ra > 0$, convection increases as Ra increases, whilst for $Ra < 0$, less heat is convected downstream for moderate values of Ra/Pe than for the forced convection solution. For all three values of Ra/Pe, however, $\bar{A}$ has a local minimum, indicating that for sufficiently great cooling (that is, Ra large and negative) there is an increase in heat transfer to the downstream wake; it appears that as the recirculation becomes sufficiently strong, this effect interacts with the forced flow to produce enhanced heat flow to the wake. An important point to emphasize here is that $\bar{A}$ does not tend to zero as $x_0 \to \infty$, a conclusion which is opposite to that reached by Robertson *et al.* (1973); however, they did not present any computed values for $\bar{A}$, which in their notation is A. In the present case, it is possible to determine for $Ra = 0$, using the solution in the Appendix and the asymptotic behaviour of the modified Bessel functions at infinity, that

$$\lim_{x_0 \to \infty} \bar{A} = \frac{1}{2}\left(\frac{Pe}{\pi}\right)^{1/2}. \tag{4.22}$$

Further computations were carried out for $Ra = 0$, $Pe = 5, 50$ using a 91×150 mesh with $x_\infty = 29.0$ and 34.8 to see if the appropriate trend could be obtained; the results are tabulated in table 2. For both values of Pe, the computed $\bar{A}$ for these values of x_∞ overestimates the analytical value by around 10%, with the appropriate asymptotic trend being more apparent only for the lower value of Pe. We would presume that a finer mesh and yet larger values of x_∞ would remedy this, although we have not pursued this here. As regards the statement that $\bar{A}$ should not tend to zero for any combination of Ra and Pe, we note that, since it is clear that this is the case when $Ra = 0$, there appears no reason to suppose that it would not hold also for $Ra \neq 0$.

Figure 5 concentrates on the $Ra < 0$ regime and documents the increase of the eddy length, L, with the value of Ra/Pe for different Pe values. We carried out additional computations for the region near $Ra/Pe = 0$ in order to ascertain whether eddies are formed for all $Ra < 0$, or whether there is a critical value above which the flow is completely attached. Although not evident from the figure, we noted that for $Pe = 1$, an eddy is formed provided $Ra/Pe < -0.8$. From the computations that were

	$x_\infty = 23.2$	$x_\infty = 29.0$	$x_\infty = 34.8$	analytical
$Pe = 5$	0.737	0.713	0.691	0.631
$Pe = 50$	2.278	2.285	2.288	1.995

TABLE 2. Comparison of $\bar{A}$ values for $Ra = 0$ for different values of x_∞, using a 91×150 mesh

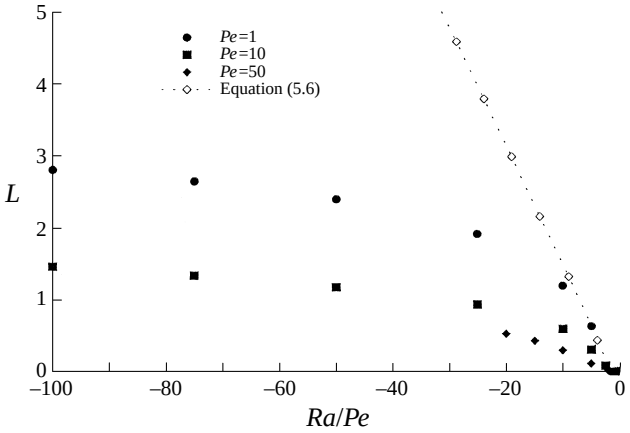

FIGURE 5. Comparison of eddy length, L, as function of Ra/Pe for $Pe = 1$, 10 and 50, with equation (5.6).

carried out for $Pe = 5$, 10, 50 and 100, it appears that the critical value for Ra/Pe is monotonically decreasing with Pe; for example, for $Pe = 100$, it was found that Ra/Pe is about -1.25. A further point here is that the leading edge of the eddy was always found to be ahead of the leading edge of the plate; this observation differs from that for a Newtonian fluid flow (Robertson *et al.* 1973), where separation and rettachment points for high enough values of the relevant dimensionless parameter (in that case Gr/Re^2, where Gr denotes the Grashof number, and Re the Reynolds number) are both at the plate surface. These issues are discussed further in the next section.

5. Discussion

Robertson *et al.* (1973) provided time-dependent computations to elucidate the mechanism for mixed convection flow separation of a viscous fluid over a short horizontal flat plate. Here, however, a mathematical explanation as to why a recirculating eddy appears for the porous media flow may be derived by considering a simplified time-independent heuristic model. It is clear that θ on $y = 0$ is essentially the linear sum of two Heaviside functions, so that $\partial\theta/\theta x$ consists of Dirac delta functions, $\pm\delta(x)$, at $x = \mp\frac{1}{2}$. Since θ is antisymmetric in y, the $\partial\theta/\theta x$ term on $y = 0$ may be thought of as the linear sum of equal and opposite vortex doublets at $x = \mp 1/2$, each of unit strength. Furthermore, we approximate the temperature field by the contribution of these doublets, so that the modified problem, reminiscent of inviscid flow theory, consists of solving for the streamfunction due to a uniform flow at infinity

and two vortex doublets; mathematically, this is expressible by

$$\nabla^2\psi = -\frac{Ra}{\pi Pe}\left(\frac{y}{(x+\frac{1}{2})^2+y^2} - \frac{y}{(x-\frac{1}{2})^2+y^2}\right), \tag{5.1}$$

subject to

$$\psi = 0 \qquad \text{on} \qquad y = 0, \tag{5.2a}$$

$$\psi \to y \qquad \text{as} \qquad y \to \infty. \tag{5.2b}$$

This is readily solved to give

$$\psi(x,y) = y\left(1 - \frac{Ra}{4\pi Pe}\log\left[\frac{(x+\frac{1}{2})^2+y^2}{(x-\frac{1}{2})^2+y^2}\right]\right); \tag{5.3}$$

a contour plot of ψ (not included here) indicates qualitative agreement for the streamfunction with the full equations, with the formation of an eddy which separates at the plate and reattaches downstream if $Ra > 0$, and reattaches at the plate having already separated upstream for $Ra < 0$. In particular, denoting by x_S and x_R the separation and reattachment positions respectively, elementary manipulation gives

$$x_S = \begin{cases} \frac{1}{2}\coth(\pi Pe/Ra) & \text{if } Ra < 0, \\ \frac{1}{2}\tanh(\pi Pe/Ra) & \text{if } Ra > 0, \end{cases} \tag{5.4}$$

$$x_R = \begin{cases} \frac{1}{2}\tanh(\pi Pe/Ra) & \text{if } Ra < 0, \\ \frac{1}{2}\coth(\pi Pe/Ra) & \text{if } Ra > 0, \end{cases} \tag{5.5}$$

with the eddy length given by

$$L = \tfrac{1}{2}\left(\coth(\pi Pe/|Ra|) - \tanh(\pi Pe/|Ra|)\right). \tag{5.6}$$

This curve has been plotted in figure 5; as one might have expected, quantitative agreement has been obtained only for small values of Ra/Pe and Pe, which is not surprising in view of the fact that the model ignores the boundary layer that is present for larger values of Ra and Pe. However, whilst these considerations are unable to say anything about, for example, the critical Ra/Pe number necessary for separation, they do mimic the fact that $-1/2 < x_R < 0$ and $x_S < -1/2$ for $Ra < 0$, as well as providing the qualitative behaviour of the eddy length as a function of Pe and Ra; for $Ra > 0$, they indicate that $0 < x_S < 1/2$ and $x_R > 1/2$, as well as showing the trend that we might have expected to see had we been able to obtain numerical solutions for higher values of Ra – a task which would presumably be possible by taking yet higher values of x_∞. In summary, therefore, it appears that the mechanism for separation of the porous medium flow is essentially the high temperature gradients at the plate edges.

6. Conclusion

In this paper, we have analysed steady mixed convection flow over a hot or cold finite horizontal flat plate embedded in a fluid-saturated porous medium. The methodology used has followed the traditional analytical–numerical approach to supply accurate results. First, based on the Darcy–Boussinesq approximation, the governing equations were given in non-dimensional form for an arbitrary body

shape. Then, an analytical solution was developed for the case when the body is symmetric, and the temperature field antisymmetric, about the horizontal axis. The resulting inner and outer composite solution was verified with the exact solution for the forced convection limit ($Ra = 0$) when the body is either a flat plate or a circular cylinder. In the rest of the paper, attention was focused on the case of a finite horizontal flat plate; detailed numerical solutions to the full governing equations were obtained by transforming to elliptical coordinates (ξ, η), defined by (4.1), and using a finite-difference scheme. Results were found for the range $1 \leqslant Pe \leqslant 100$, $|Ra| \leqslant 10^3$. All the results were checked for accuracy very carefully by varying the grid size. Numerical results were also compared (see table 1) with those of Cheng (1977) and Prasad *et al.* (1988) for a similar problem in the forced convection limit, and found to agree well, particularly for large values of Pe.

Perhaps the most significant result for the present problem is the formation of separation eddies for both heating and cooling cases and high enough values of Ra. For $Ra/Pe > 0$, the flow accelerates near the plate, and a separation bubble appears towards the trailing edge, which reattaches to the x-axis further downstream. For $Ra/Pe < 0$, we found that the buoyancy-induced streamwise pressure gradient also causes the flow to separate, and a recirculating eddy develops adjacent to the plate surface. For $Pe = 1$, this eddy forms for $Ra/Pe < -0.8$, while for $Pe = 100$, $Ra/Pe < -1.25$; further computations for $1 \leqslant Pe \leqslant 100$ indicated that the critical value of Ra/Pe is monotonically decreasing with Pe. An additional point here is that the leading edge of the eddy was always found to be ahead of the leading edge of the plate, a result which differs from that for a viscous (non-porous) medium (see Robertson *et al.* 1973). Furthermore, there are several indications why it is unlikely that the appearance of the separating eddies would be a numerical artefact of the implementation of the chosen boundary conditions. The appearance of reverse flow as $|Ra|/Pe$ increases in fact seems quite natural, especially in the absence of fluid inertia, because the pressure force due to buoyancy increases in magnitude and opposes the forced flow (over the plate when $Ra < 0$ and downstream of the plate when $Ra > 0$). Note that separation in porous media mixed convection has been reported elsewhere (Pop, Lesnic & Ingham 1995), albeit for a different flow configuration.

It is worth, in conclusion, considering the use of elliptical coordinates in this work in the wider context of boundary-layer theory in porous media. The advantage of these coordinates is that the region near the plate is effectively magnified, particularly the singular regions near the ends of the plate. In this respect, we mention also that Rees & Bassom (1991) provided a method for studying free convection from a vertical or horizontal semi-infinite surface buried in a porous medium using parabolic coordinates; in that case, the full nonlinear governing equations were reduced to a set of ordinary differential equations which are, in fact, identical to those found by Cheng & Minkowycz (1977) and Cheng & Chang (1976).

A considerable qualitative difference has now been found to exist between buoyancy-induced flows from a short vertical and a horizontal surface placed in a fluid-saturated porous medium. An interesting extension to these problems, of some importance, is to determine how their dissimilar flow characteristics can be reconciled by examining the buoyancy-induced flow along an inclined short flat plate embedded in a porous medium, using the same procedure as that adopted for the present configuration.

The authors wish to thank the referees for their comments on an earlier version of the paper. M.V. gratefully acknowledges the financial support of the European Union.

Appendix. Solution for forced convection ($Ra = 0$)

When $Ra = 0$, $\psi \equiv y$, so that the steady heat equation reduces to

$$\frac{\partial \theta}{\partial x} = \frac{1}{Pe}\left(\frac{\partial^2 \theta}{\partial x^2} + \frac{\partial^2 \theta}{\partial y^2}\right), \tag{A 1}$$

subject to

$$\theta = 0 \qquad \text{on} \qquad y = 0, \quad |x| > \tfrac{1}{2}, \tag{A 2a}$$

$$\theta = 1 \qquad \text{on} \qquad y = 0, \quad |x| \leqslant \tfrac{1}{2}, \tag{A 2b}$$

$$\theta \to 0 \qquad \text{as} \qquad (x^2 + y^2)^{1/2} \to \infty. \tag{A 2c}$$

To proceed to a closed-form solution for θ, writing $\theta(x, y) = \mathrm{e}^{\lambda x} F(x, y)$, where $\lambda = Pe/2$, yields a Helmholtz equation for F,

$$\frac{\partial^2 F}{\partial x^2} + \frac{\partial^2 F}{\partial y^2} = \lambda^2 F, \tag{A 3}$$

subject to

$$F = 0 \qquad \text{on} \qquad y = 0, \quad |x| > \tfrac{1}{2}, \tag{A 4a}$$

$$F = \mathrm{e}^{-\lambda x} \qquad \text{on} \qquad y = 0, \quad |x| \leqslant \tfrac{1}{2}, \tag{A 4b}$$

$$F \to 0 \qquad \text{as} \qquad (x^2 + y^2)^{1/2} \to \infty. \tag{A 4c}$$

Equation (A 3), subject to (A 4*a–c*) is solved by the method of Fourier transforms to give

$$\theta(x, y) = \frac{\mathrm{e}^{\lambda x}}{\pi} \int_{-\infty}^{\infty} \frac{\sinh \tfrac{1}{2}(\lambda + \mathrm{i}s)\, \mathrm{e}^{-(\lambda^2 + s^2)^{1/2} y + \mathrm{i}sx}}{\lambda + \mathrm{i}s}\, \mathrm{d}s, \tag{A 5}$$

which is easily shown to be real. A little more manipulation gives the results necessary for § 4.1:

$$-\frac{\pi}{\lambda}\left(\frac{\partial \theta}{\partial y}\right)_{y=0} = \begin{cases} \mathrm{e}^{x_+}\,[K_0(-x_+) - K_1(-x_+)] & \\ \quad -\mathrm{e}^{x_-}\,[K_0(-x_-) - K_1(-x_-)] & \text{if } x < -\tfrac{1}{2}, \\ \mathrm{e}^{x_+}\,[K_0(x_+) + K_1(x_+)] & \\ \quad -\mathrm{e}^{x_-}\,[K_0(-x_-) - K_1(-x_-)] & \text{if } -\tfrac{1}{2} < x < \tfrac{1}{2}, \\ \mathrm{e}^{x_+}\,[K_0(x_+) + K_1(x_+)] & \\ \quad -\mathrm{e}^{x_-}\,[K_0(x_-) + K_1(x_-)] & \text{if } x > \tfrac{1}{2}, \end{cases} \tag{A 6}$$

where

$$x_+ = \lambda(x + \tfrac{1}{2}) \qquad \text{and} \qquad x_- = \lambda(x + \tfrac{1}{2}),$$

and K_0 and K_1 are the modified Bessel functions.

REFERENCES

Aldoss, T. K., Chen, T. S. & Armaly, B. F. 1993*a* Nonsimilarity solutions for mixed convection from horizontal surfaces in a porous medium – variable surface heat flux. *Intl J. Heat Mass Transfer* **36**, 463–470.

Aldoss, T. K., Chen, T. S. & Armaly, B. F. 1993*b* Nonsimilarity solutions for mixed convection from horizontal surfaces in a porous medium – variable wall temperature. *Intl J. Heat Mass Transfer* **36**, 471–477.

Aldoss, T. K., Chen, T. S. & Armaly, B. F. 1994 Mixed convection over nonisothermal horizontal surfaces in a porous medium – the entire regime. *Numer. Heat Transfer* A **25**, 685–701.

Aldoss, T. K., Jarrah, M. A. & Duwari, H. M. 1994 Wall effect on mixed convection flow from horizontal surfaces with a variable heat flux. *Can. J. Chem. Engng* **72**, 35–42.

Bejan, A. 1984 *Convective Heat Transfer*. Wiley.

Bejan, A. 1987 Convective heat transfer in porous media. In *Handbook of Single-Phase Convective Heat Transfer* (ed. S. Kakac, R. K. Shah & W. Aung), pp. 16.1–16.34. J. Wiley and Sons.

Carrier, G. F., Krook, M. & Pearson, C. E. 1983 *Functions of a Complex Variable*. Hod Books, Ithaca, New York.

Chang, I.-D. 1961 Navier–Stokes solutions at large distances from a finite body. *J. Math. Mech.* **10**, 811–876.

Cheng, P. 1977 Similarity solutions for mixed convection from horizontal impermeable surfaces in saturated porous media. *Intl J. Heat Mass Transfer* **20**, 893–898.

Cheng, P. & Chang, I.-D. 1976 Buoyancy induced flows in a saturated porous medium adjacent to impermeable horizontal surfaces. *Intl J. Heat Mass Transfer* **19**, 1267–1272.

Cheng, P. & Minkowycz, W. J. 1977 Free convection about a vertical flat plate embedded in a porous medium with application to heat transfer from a dike. *J. Geophys. Res.* **82**, 2040–2044.

Higuera, F. J. & Weidman, P. D. 1995 Natural convection beneath a downward facing heated plate in a porous medium. *Eur. J. Mech.* B *Fluids* **14**, 29–40.

Kakac, S., Kilkis, B., Kulacki, F. A. & Arinc, F. (ed.) 1991 *Convective Heat and Mass Transfer in Porous Media*. Kluwer.

Kimura, S., Bejan, A. & Pop, I. 1985 Natural convection near a cooled plate facing upward in a porous medium. *J. Heat Transfer* **107**, 819–825.

Kimura, S. & Pop, I. 1992 Conjugate free convection from a circular cylinder in a porous medium. *Intl J. Heat Mass Transfer* **35**, 3105–3113.

Kimura, S. & Pop, I. 1993 Conjugate natural convection from a horizontal cylinder. *Numer. Heat Transfer* **25**, 347–361.

Kimura, S. & Pop, I. 1994 Conjugate free convection from a sphere in a porous medium. *Intl J. Heat Mass Transfer* **37**, 2187–2192.

Lai, F.-C. & Kulacki, F. A. 1990 The influence of surface mass flux on mixed convection from horizontal surfaces in a porous medium – variable surface heat flux. *Intl J. Heat Mass Transfer* **33**, 576–579.

Merkin, J. H. & Needham, D. J. 1987 The natural convection flow above a heated wall in a saturated porous medium. *Q. J. Mech. Appl. Maths* **40**, 559–574.

Merkin, J. H. & Pop, I. 1989 Free convection above a horizontal circular disk in a saturated porous medium. *Wärme- und Stoffübertr.* **24**, 53–60.

Nakayama, A. 1995 *PC-Aided Numerical Heat Transfer and Convective Flow*. CRC Press.

Nield, D. A. & Bejan, A. 1992 *Convection in Porous Media*. Springer.

Oosthuizen, P. H. 1988 Mixed convective heat transfer from a heated horizontal plate in a porous medium near an impermeable surface. *J. Heat Transfer* **110**, 390–394.

Patankar, S. V. 1980 *Numerical Heat Transfer and Fluid Flow*. Hemisphere.

Pop, I., Lesnic, D. & Ingham, D. B. 1995 Conjugate mixed convection on a vertical surface in a porous medium. *Intl J. Heat Mass Transfer* **38**, 1517–1525.

Prasad, V., Lai, F.-C. & Kulacki, F. A. 1988 Mixed convection in horizontal porous layers heated from below. *J. Heat Transfer* **110**, 395–402.

Rees, D. A. S. & Bassom, A. P. 1991 Some exact solutions for free convective flows over heated semi-infinite surfaces in porous media. *Intl J. Heat Mass Transfer* **34**, 1564–1567.

Robertson, G. E., Seinfeld, J. H. & Leal, L. G. 1973 Combined forced and free convection flow past a horizontal flat plate. *AIChE J.* **19**, 998–1008.

Vynnycky, M. & Kimura, S. 1994 Conjugate free convection due to a vertical plate in a porous medium. *Intl J. Heat Mass Transfer* **37**, 229–236.

Vynnycky, M. & Kimura, S. 1995 Transient conjugate free convection due to a vertical plate in a porous medium. *Intl J. Heat Mass Transfer* **38**, 219–231.

Vynnycky, M. & Kimura, S. 1996 Conjugate free convection due to a heated vertical plate. *Intl J. Heat Mass Transfer* **39**, 1067–1080.